Progress in Organic Coatings 131 (2019) 407–416

Contents lists available at ScienceDirect

Progress in Organic Coatings

journal homepage: www.elsevier.com/locate/porgcoat

Improvement of the corrosion protection of polypyrrole coating for CT3 mild steel with 10-camphorsulfonic acid and molybdate as inhibitor dopants

Ha Manh Hung[a], Duong Khanh Linh[b], Nguyen Thuy Chinh[c], Le Minh Duc[d], Vu Quoc Trung[b,*]

[a] Faculty of General Education, Hanoi University of Mining and Geology, Duc Thang Ward, Bac Tu Liem District, Hanoi, 100000, Vietnam
[b] Faculty of Chemistry, Hanoi National University of Education, No. 136 Xuan Thuy Road, Cau Giay District, Hanoi, 100000, Vietnam
[c] Institute for Tropical Technology, Vietnam Academy of Science and Technology, No. 18 Hoang Quoc Viet Street, Cau Giay District, Hanoi, 100000, Vietnam
[d] Sub-Institute of Occupational Safety and Health & Environmental Protection in Central of Vietnam, No. 178 Trieu Nu Vuong, Hai Chau District, Da Nang, 552200, Vietnam

ARTICLE INFO

Keywords:
10-camphorsulfonic acid
Polypyrrole coating
Corrosion protection
Molybdate anion dopant
CT3 mild steel

ABSTRACT

This paper presents the doping influence of both molybdate anion and 10-camphorsulfonic acid (CSA) on the characterization and corrosion protection properties of polypyrrole (PPy) film prepared on passivized CT3 mild steel. The effect of CSA and molybdate anion concentrations on the properties and morphology of PPy film was characterized by Raman, FTIR, EDX and SEM methods. The doping of both CSA and molybdate anion into the PPy film can lead to an increase in the thermal stability and redox properties of the PPy film. The PPy film doped with both CSA and molybdate anion displayed excellent anti-corrosion ability for CT3 mild steel in comparison with the PPy film and PPy film doped with only CSA or molybdate anion. Furthermore, the salt spray test was also carried out to more effectively evaluate the corrosion protection of doped PPy film for mild steel.

1. Introduction

Recently, conducting polymers (CPs), such as polyaniline (PANi) [1–3], poly(amido-amine) [3,4], polypyrrole (PPy) [5–7], and poly acrylamide [8], which are applied for the corrosion protection of metals and alloys because of their superior effectiveness against corrosion, have been a focus of studies. They are synthesised easily with less toxic chemicals in the electrochemical process – a popular method for the synthesis of CPs. The coating of CPs on the surface of metallic substances can limit the corrosion of many materials, such as aluminum, iron, magnesium, and mild steel. The protective ability of the CP coating can be explained by the formation of a shielding layer to stop the attack of corrosive agents, known as the barrier effect [9]. On the other hand, CPs may be reflected as a protective anode because a CP film exists in the oxidized form, which makes the steel passive with a high open circuit potential [2,10]. Here, the role of the dopant anion is quite large. When the corrosive agent penetrates through the defects on the films, the substrate metal will be corroded. Due to galvanic coupling, the CP film is reduced to provide dopant anions at those corrosion sites. The released anions can combine with the metallic cations to form insoluble compounds on the surface of the steel, resulting in the protection of the steel. CPs have shown self-healing protection in this way.

Among the CPs, both PANi and PPy are common CPs for the corrosion protection of metals and alloys. Although PANi has many advantages, such as good anti-corrosion protection [1,2] and low cost, the high toxicity of PANi has limited its applications in industry and life. In contrast, PPy is an environmentally friendly material with good corrosion resistance [11–13]. That is, a thin-layer PPy film can be formed on a metallic surface, therefore protecting the metal for a long time [14].

Several studies have reported the good corrosion inhibition of PPy films on pure iron [15,16], mild steel [17–19], and stainless steel [2,20,21]. Actually, PPy cannot offer complete anodic protection for iron [22–24]. Therefore, dopant anions, such as sodium *bis*(2-ethylhexyl)sulfosuccinate [5,25,26], molybdate, phosphomolybdate, naphthalenedisulfonate, dihydroxynaphthalenedisulfonate, anthraquinonedisulfonate, and dodecylsulfate ions [18,27,28], have been used to improve the protective properties of PPy. The dopants could be added into the polymers by chemical or electrochemical methods in one step (simultaneous polymerization and dopants synthesis) or multiple steps. Some large-molecule organic acids, such as camphorsulfonic acid (CSA), benzenesulfonate (BS), and *p*-toluenesulfonate, are more suitable than sulfuric or phosphoric acid for improving the anti-corrosive performance of coatings [29–33]. For instance, a PPy coating doped with CSA exhibited good solubility and an enhancement of the

* Corresponding author.
E-mail address: trungvq@hnue.edu.vn (V.Q. Trung).

https://doi.org/10.1016/j.porgcoat.2019.03.006
Received 30 June 2018; Received in revised form 4 March 2019; Accepted 4 March 2019

Table 1
Abbreviated samples and composition of the polymerization solutions.

Samples or solution	$C_{10}H_{16}O_4S$ (CSA)	Na_2MoO_4	Pyrrole (Py)	pH
P1	0.025 M	–	0.1 M	1.72
P2	0.05 M	–	0.1 M	1.48
P3	0.1 M	–	0.1 M	1.27
P4	0.05 M	0.01 M	0.1 M	1.48
P5	0.05 M	0.02 M	0.1 M	1.48
P6	0.05 M	0.03 M	0.1 M	1.48

electrical conductivity [31]. Furthermore, a CSA-doped PPy coating could have potential application in the sensor field. Jiang et al. [32] concluded that a PPy/CSA coating on 304SS bipolar plates displayed low current density and low interfacial contact resistance (ICR) values in comparison with PPy and PPy-SO_4^{2-} coatings. The PPy/CSA coating had a less rough surface without micro cracks and a superior anti-corrosive performance during a 660-hour immersion test in the simulated environment of proton-exchange membrane fuel cells (PEMFC). CSA-doped PANi has also exhibited a positive effect for anti-corrosive coating [34–36]. Zhihao Chen et al. prepared molybdate-doped PPy in an oxalic acid medium for the corrosion protection of carbon steel in 0.1 M HCl solution [18]. The corrosion protection performance of molybdate-doped PPy coated steel in 0.1 M HCl solution was investigated by electrochemical impedance spectroscopy and Tafel polarization. Molecular dynamics simulations were engaged to assess the interactions between the metal surface and complex coatings. The exceptional anti-corrosion performance of the molybdate-doped PPy coating was associated with the complex passive film on the metal surface and the barrier effect of the coating. However, the consecutive doping of CSA and molybdate anion in a PPy matrix for corrosion protection and improvement of the conductivity of mild steel is infrequently reported.

In our previous publications, molybdate anions were used as an inhibitor for PPy films prepared in oxalic acid and succinic acid [32,37,38]. The results confirmed that the presence of molybdate anions and oxalic acid or succinic acid resulted in an improvement in the anti-corrosive property of the PPy film. Some properties of the PPy doped with molybdate and succinate, such as the composition, morphology, structure, and thermal stability, as well as the corrosion protection ability (OCP, Tafel, EIS), were discussed. However, the cyclic voltammogram (CV) and salt spray stability of these films have not been investigated. Moreover, the effect of CSA and molybdate on the PPy film could be different from that of succinic acid and molybdate on the PPy film due to differences in the structures of the acid dopants (succinic acid has a linear structure while CSA has a spatial one). Nautiyal et al. found that the type and size of the dopants (short chain or long chain) could strongly affect the protection performance of the coating against chloride ion attack on the metal surface [39]. Therefore, this paper examined the effect of doping both CSA and molybdate anions in PPy film on the corrosion protection ability of the PPy film coating on CT3 mild steel, combining the advantages of the large-sized CSA ions and the strong anticorrosion ability of molybdate anions. It is expected that doping both CSA and molybdate anions into the PPy matrix could yield a promising corrosion protection coating.

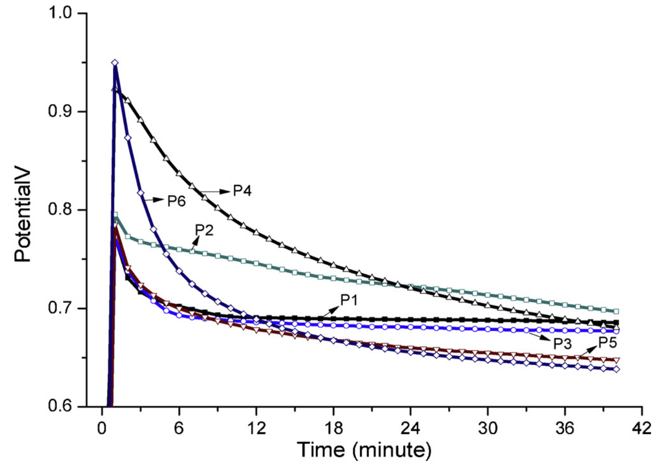

Fig. 2. The polarization curves vs. time of electropolymerization of PPy in different dopant solutions.

2. Experimental

2.1. Chemicals and materials

Pyrrole (Py) monomer (reagent grade, 98%), $Na_2MoO_4{\cdot}2H_2O$ (98%) and 10-camphorsulfonic acid (CSA, 99%) were obtained from Merck Co., and the other reagents were used as received without any further purification. CT3 mild steel (TISCO com., Thai Nguyen, Vietnam, Mn: 0.62%; C: 0.16%; Si: 0.15%; S: 0.042%; and P: 0.010%, according to GOST 001-2001-TCVN 1656-75 standard) was purchased in the market with a size of 13.5 mm x 13.5 mm x 2 mm. The CT3 steels were polished and cleaned by ethanol and distilled water.

2.2. Synthesis of doped PPy film on CT3 mild steel

The doped PPy film on CT3 mild steel was prepared as follows: first, the CT3 steel substrate was polished, washed with acetone solvent, and

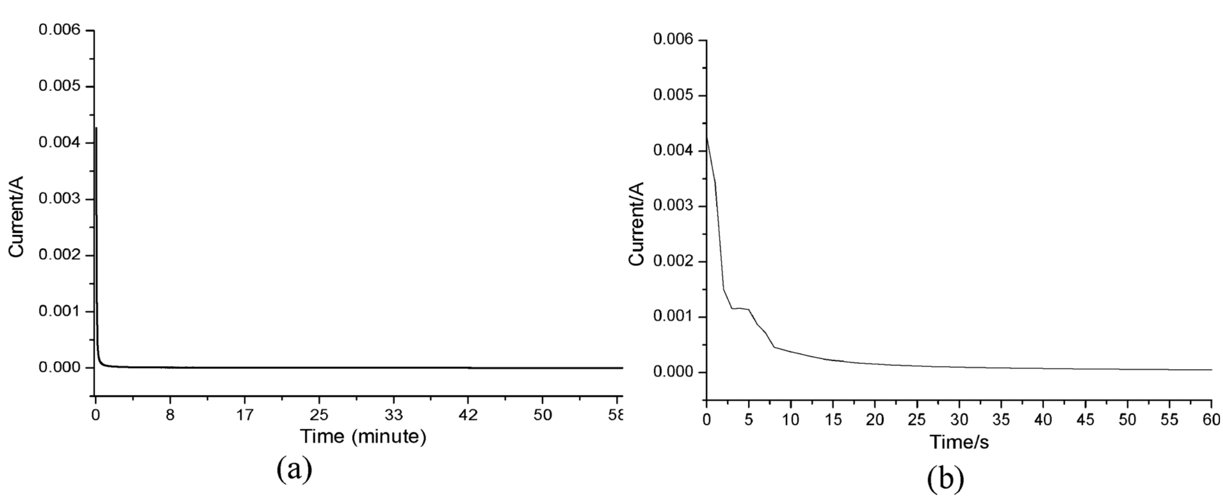

Fig. 1. The current density curve vs. time for CT3 mild steel in 0.1 M Na_2MoO_4 solution at +0.5 V for 60 min (a) and during the first minute (b) of the polarization.

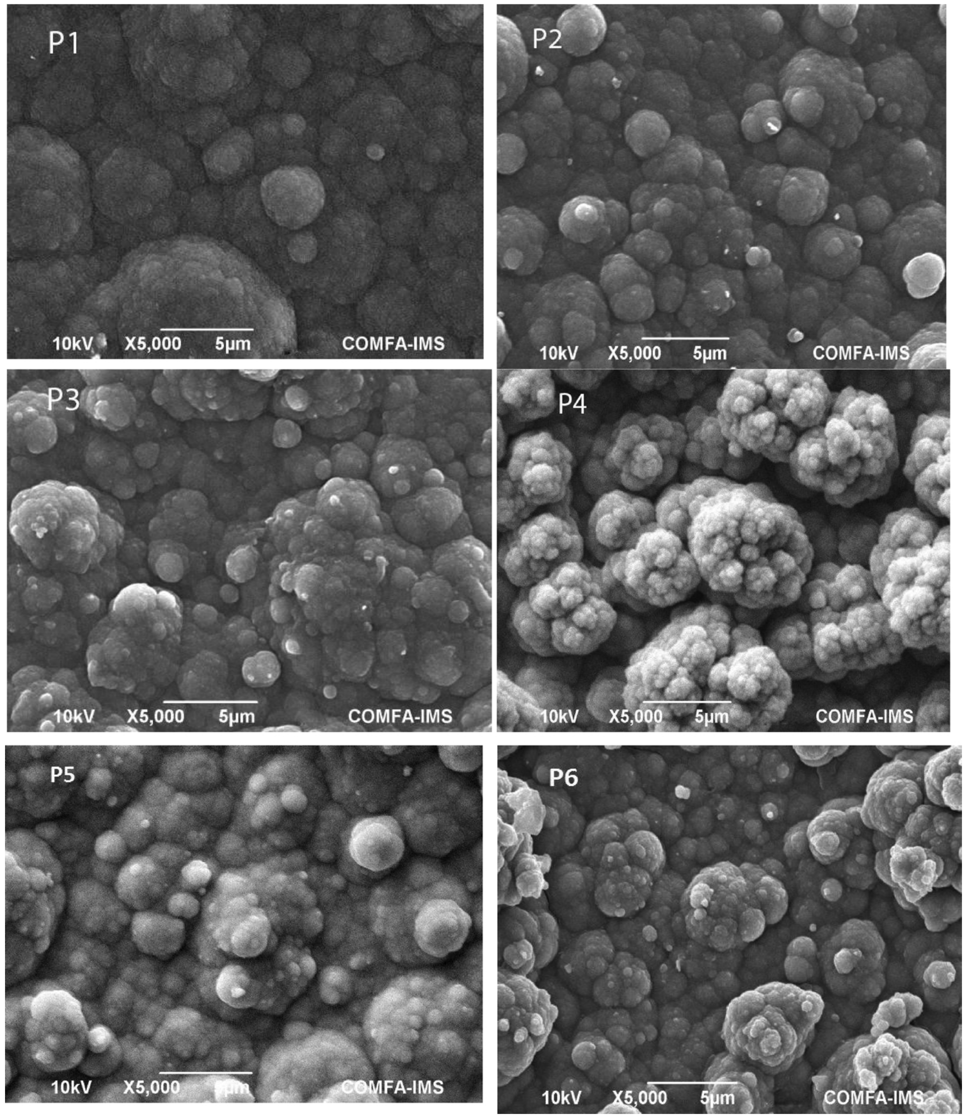

Fig. 3. SEM images of doped PPy films on the surface of CT3 mild steel.

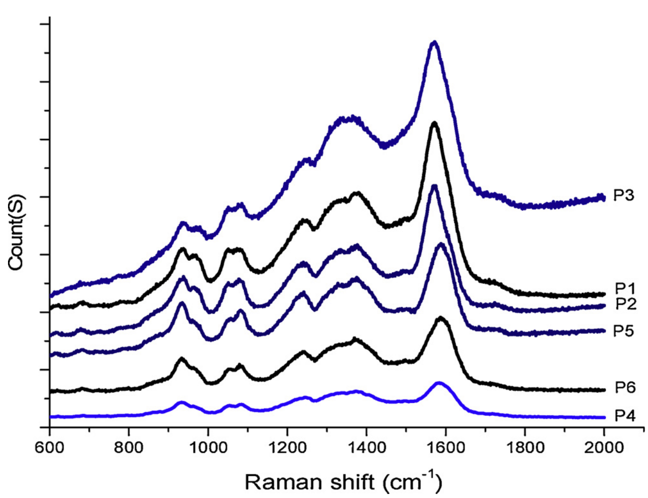

Fig. 4. Raman spectra of doped PPy films.

then passivated electrochemically in 0.1 M Na_2MoO_4 solution at + 0.5 V (Ag/AgCl) for 60 min. The sample was then washed with distilled water and kept in a nitrogen atmosphere for storage. Second, the treated CT3 steel sample was electropolymerized with PPy with a constant current of 0.9 mA/cm^2 for 50 min in a homogeneous solution of pyrrole monomer and CSA dopant anions. After that, the obtained PPy film was washed many times with distilled water and dried at 50 °C in vacuum. The PPy film doped with both CSA and MoO_4^{2-} was electropolymerized with the same 2-step process mentioned above. The obtained samples prepared with different concentrations of CSA, sodium molybdate and different pH solutions are listed in Table 1. The first 3 samples (P1, P2 and P3) were used to find the most suitable concentration of CSA in the electrolyte. Then, samples P4, P5, and P6 were prepared with different sodium molybdate concentrations to evaluate the effectiveness of both CSA and molybdate anions on the properties and corrosion protection of PPy film on CT3 mild steel.

2.3. Characterization of PPy film

Examination of the surface morphology and element analysis of the doped PPy films were carried out using a HITACHI-4800 FESEM device (Japan) and energy dispersive X-ray analysis (EDX). Fourier transform infrared (FT-IR) spectra of the samples were recorded on a Prestige -21 (Shimadzu) at room temperature with a resolution of 4 cm^{-1} and averaging 16 scans with wavenumbers of 400 - 4000 cm^{-1}. The chemical structure of PPy and doped PPy films was characterized by

Table 2
Raman shift (cm^{-1}) of theoretical PPy (a) [40], practical PPy (b) [41] and doped PPy films.

Theoretical PPy (a)	Experimental PPy (b)	P1	P2	P3	P4	P5	P6	Vibration
1676	1589	1572	1572	1574	1585	1590	1590	$\upsilon_{C=C}$
1307	1328	1376	1381	1372	1368	1368	1368	$\upsilon_{C\text{-}N}$
–	–	1231	1224	1230	1231	1231	1236	$\delta_{C\text{-}C}$
1049	1047	1047	1067	1087	1080	1080	1080	$\delta N\text{-}_H$
955	976	939	931	935	931	932	933	δ ring deformation

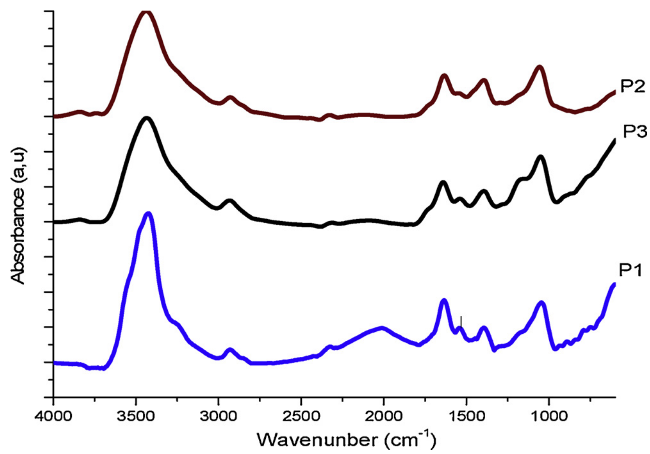

Fig. 5. IR spectra of P1, P2, and P3.

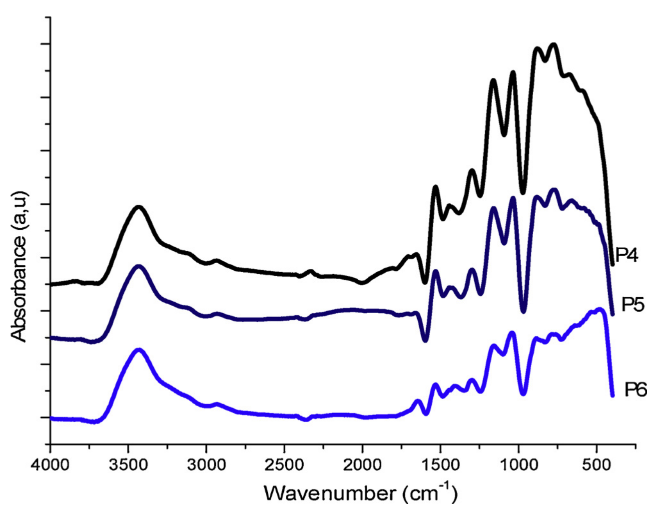

Fig. 6. IR spectra of P4, P5, and P6.

Raman spectroscopy on a Laser Raman Spectrophotometer (Ramalog 9I, USA). The thermal properties of the samples were examined on a TGA-50H thermogravimetric analyzer (Shimadzu) from room temperature to 800 °C at a heating rate of 5 °C/min under an argon atmosphere.

The electrochemical experiments were carried out with a Zennium Potentiostat/Galvanostat/Electrochemical Impedance Spectroscopy (EIS) instrument (Germany). A conventional three-electrode cell with a Pt gauze counter electrode and a Ag/AgCl reference electrode was used. The OCP of all the samples were recorded in 3% NaCl solution. Cyclic voltammetry measurements were used to study the redox property of PPy in free monomer solution with a scan rate of 10 V/s. The EIS spectra of PPy were recorded in 3% NaCl solution with an amplitude of 5 mV AC on a DC potential between 100 kHz and 0.1 Hz at open circuit potential. The potentio-dynamic polarization measurement was carried out at a sweep rate of 1 mV s^{-1} in 3% NaCl solution.

A salt spray test was also conducted to test the stability of the doped PPy film in 50 mg/l NaCl at a temperature of 35 °C and a pressure of 100 kPa. These conditions were controlled in a Q-FOG CCT 600 salt spray test instrument.

All the measurement results were expressed as the means of three independent experiments.

3. Results and discussion

3.1. Electropolymerization of doped PPy on CT3 mild steel

3.1.1. Surface passivation of CT3 mild steel

To obtain a thin PPy film with good adhesion, smoothness and gloss on the surface of the substrate, CT3 mild steel samples were polarized in 0.1 M Na_2MoO_4 solution for 60 min at +0.5 V (Ag/AgCl) before electropolymerization [37]. The curve of the current density vs. the polarization time of a CT3 mild steel sample is shown in Fig. 1a.

It can be seen in Fig. 1b that the current density decreased suddenly from 415 μA to 5 μA after 60 s of polarization. From the inflection point at 60 s, the current density of the sample is nearly zero. This means that a passivated layer on the sample was formed.

3.1.2. Synthesis of doped PPy films on CT3 mild steel

The potential vs. time curves of doped PPy films (on CT3 steel) synthesized at a current density of 0.9 mA/cm^2 in a solution containing different concentrations of CSA and 0.1 M pyrrole monomer with and without molybdate anions (Table 1) are expressed in Fig. 2.

The obtained PPy films were thin, smooth, black and homogeneous. The behavior of passivized CT3 steel looked like an inert electrode. PPy was formed on it without any difficulties. The P1, P2, P3, and P4 samples have a similar potential of PPy polymerization, approximately 0.75 V (Ag/AgCl). On the other hand, the P5 and P6 samples exhibited a lower oxidation potential than the others, near 0.65 V. This can be explained as follows: at a higher content of MoO_4^{2-}, the P5 and P6 samples displayed a slower formation rate, so they had a more homogeneous surface, leading to a decrease in the oxidized potential. In addition, hydrogen bonding between the SO_3H group in CSA and the NH group in PPy could also affect the formation rate of the doped PPy films.

3.2. Morphology of doped PPy films

The morphology of doped PPy films with and without molybdate anion and CSA dopants is demonstrated in Fig. 3. It is observed that doped PPy films consisted of a typical structure with homogeneously distributed cauliflower-shaped particles as mentioned in Refs. [15,34,38]. The dense cauliflower structure of the film was better for the corrosion protection of the metal. The simultaneous presence of CSA and molybdate anions does not cause a change in the morphology of PPy films. It seemed that the film had a thicker, rougher and clearer cauliflower shape in the presence of molybdate anion (P4, P5 and P6 samples, Fig. 3). This will help to enhance the effectiveness of the protection corrosion for CT3 steel of P4, P5 and P6 samples as will be discussed below.

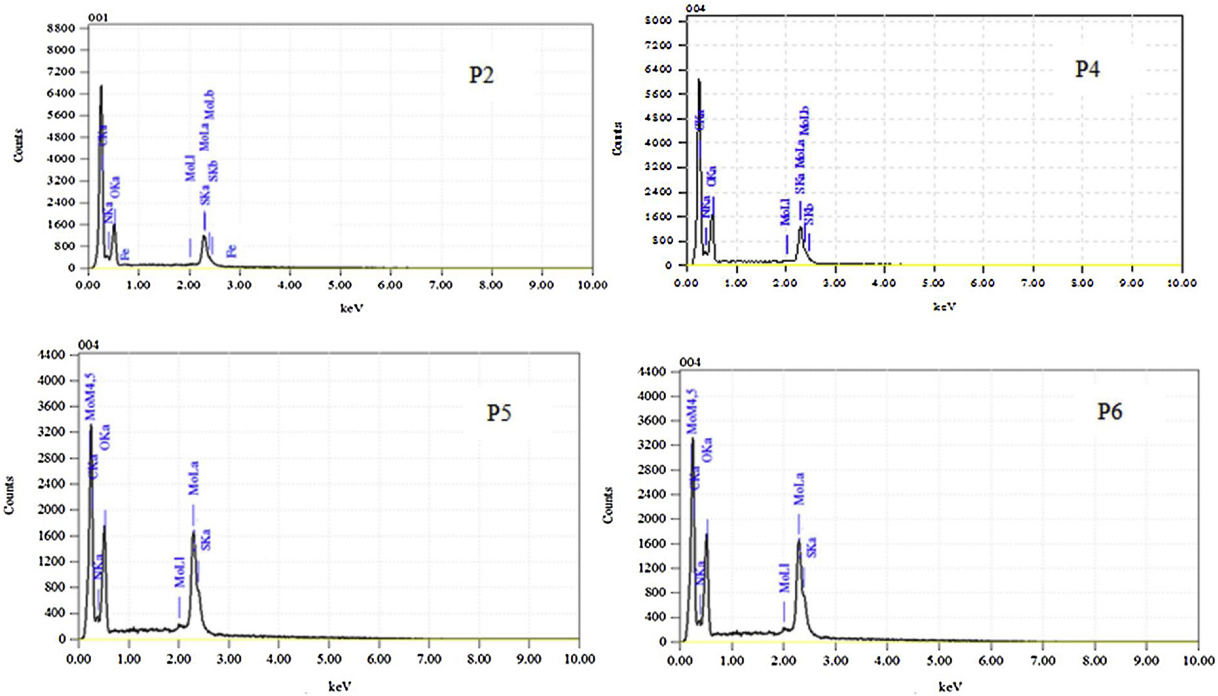

Fig. 7. EDX spectra of P2, P4, P5, and P6.

Table 3
Element analysis results of P2, P4, P5 and P6.

Element (%)	P2	P4	P5	P6
C	65.75	28.62	18.80	17.30
N	11.87	15.59	3.61	4.46
O	15.35	17.77	23.02	20.12
S	6.71	2.60	2.19	1.78
Mo	–	35.43	52.38	56.34
Fe	0.32	–	–	–
Total (%)	100	100	100	100

3.3. Raman spectra of PPy doped films

Fig. 4 presents the Raman spectra of the CSA-PPy and MoO_4^{2-}-CSA-PPy films. It can be seen that PPy was in an oxidized state and that there is a slight difference from the Raman shift in the Raman spectra of doped PPy films synthesized under different conditions (Fig. 4 and Table 2). This result may agree with the polarization potential of PPy films as discussed before in terms of the existence of physical interaction in doped PPy films. For instance, the peaks with a strong intensity from 1572 to 1590 cm^{-1} characterized the stretching of conjugative backbone C—C═C, while the peaks at 1368-1381 cm^{-1} corresponded to N—C ring stretching. The peaks related to —N—H in-plane bending, and C—C stretching were found at 1047–1080 cm^{-1} and 1224–1236 cm^{-1}, respectively [34,35]. The peaks at 931–939 cm^{-1} were attributed to ring deformation and —C—H out of plane deformation [36]. To compare with the Raman data of oxidized PPy which were calculated according to theory [40] and practice (in PPy/Al_2O_3 nanocomposite) [40], the specific value in the Raman spectra of doped PPy films is catalogued in Table 2. The Raman shift of CSA-PPy and MoO_4^{2-}-CSA-PPy films is different from the theoretical and experimental data for PPy. Furthermore, the presence of CSA in the doped PPy films is exhibited by the appearance of the C—C stretching vibration, which is absent in the theoretical and experimental PPy data.

3.4. FTIR spectra of doped PPy films

From Figs. 5 and 6, the appearance of —NH, —CH, —C═O, —C═C, —C═N, and —SO groups of PPy and CSA structures in the FTIR spectra of the P1-P6 samples can be seen. The stretching vibrations of the N—H bond in the aromatic vibration ($\upsilon_{N\text{-}H}$) of PPy or O—H bond in the water molecule were assigned at 3425 cm^{-1} (P1), 3437 cm^{-1} (P2-P5), and 3431 cm^{-1} (P6). The peak at 2931 cm^{-1} (P1–P6) was assigned as the C—H stretching vibration. The vibration of the C═O bond ($\upsilon_{C=O}$) could be seen at 1635 cm^{-1} (P1), 1631 cm^{-1} (P2), 1639 cm^{-1} (P3), 1654 cm^{-1} (P4, P5), and 1647 cm^{-1} (P6). $\upsilon_{C=C\ aromatic}$, $\upsilon_{C=N}$ could be given at 1543 cm^{-1} (P1), 1550 cm^{-1} (P2), 1539 cm^{-1} (P3), and 1531 cm^{-1} (P4, P5, P6). The band approximately 1392 cm^{-1} (P1), 1396 cm^{-1} (P2, P3), and 1430 cm^{-1} (P4-P6) was attributed to the vibration of N—H ($\delta_{N\text{-}H}$) or O—H ($\delta_{O\text{-}H}$). The bands of 1045 cm^{-1} (P1), 1053 cm^{-1} (P2, P3), 1033 cm^{-1} (P4, P5), and 1041 cm^{-1} were attributed to the —SO group. The peaks at 840 and 896 cm^{-1} (P4, P5, P6) could be attributed to the $(MoO_4)^{2-}$ moiety. The peak at 1033-1053 cm^{-1} was contributed to the electrostatic interaction of $N—H^+$ in PPy with > S═O— in CSA [28]. The slight shift in the N—H bending and C═O stretching vibrations is an evidence of the above electrostatic interaction. These results suggested that the doping of both CSA and MoO_4^{2-} with PPy electrochemically was successful.

3.5. EDX analysis of doped PPy films

To confirm the successful doping of both MoO_4^{2-} and CSA, the EDX spectra were recorded to determine the composition of elements in the doped PPy films. The P2, P4, P5 and P6 samples were prepared at the same content of CSA, so we determined the EDX spectra for only these samples for an easier comparison. Fig. 7 and Table 3 present the EDX spectra and the atomic percentages of elements in the doped PPy films. It can be seen that there existed 5 elements (C, O, S, N, Mo) in P4, P5, and P6, while Mo was absent, and Fe was present in P2. The absence of Mo in P2 strongly supported the hypothesis that molybdate in the passive layer could not act as a dopant of PPy. The layer could not be dissolved by the polarization, becoming an anion in the electrolyte. The molybdate of this passive layer was stable enough during the

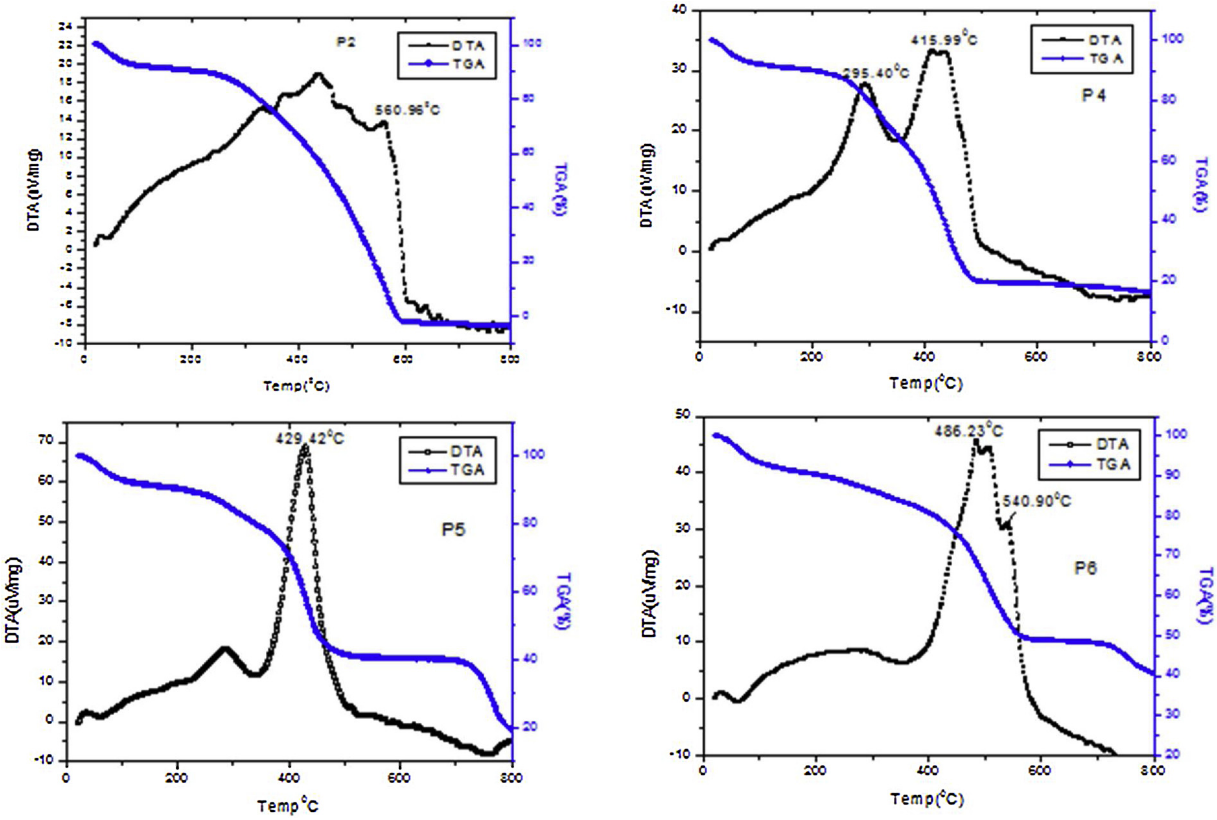

Fig. 8. TGA diagrams of the samples P2, P4, P5, and P6.

Table 4
The remained weight of P2, P4, P5, and P6 samples at different temperatures.

Temp. (°C)		≤ 200	200–400	400–600	> 600
Remained weight (%)	P2	90.22	85.12	0.344	0
	P4	89.90	60.63	19.43	15.94
	P5	90.33	75.24	42.37	19.90
	P6	90.30	80.58	48.91	40.33

electropolymerization of Py. In contrast to P2, for the samples P4, P5 and P6, molybdate was detected as a dopant in the polymer film. The molybdate anions were mobile enough to insert into the polymer as a dopant. Interestingly, the appearance of S in the P4, P5, and P6 films also confirms that both MoO_4^{2-} and CSA were doped simultaneously into the PPy film. The content of Mo increased when the Na_2MoO_4 concentration was increased, while the S content decreased. This could confirm that the existence of competition between CSA and MoO_4^{2-} in doping process depended on the kinds of ions. This result proved that the MoO_4^{2-}-CSA-PPy coatings for CT3 also exhibited a better protection compared with the PPy films doped with succinic acid and MoO_4^{2-} which were investigated in Ref. [38]. The MoO_4^{2-} and CSA doping yield reduced with the increase of the MoO_4^{2-} concentration. This can be explained by the rate of the PPy polymerization reaction. To our knowledge, PPy needs to be formed together with both MoO_4^{2-} and CSA to give a thin film on the surface of CT3 mild steel. Here, the decline in the content of C and N is easily observed when raising the MoO_4^{2-} concentration, corresponding to the polymerization process occurring more slowly in this case.

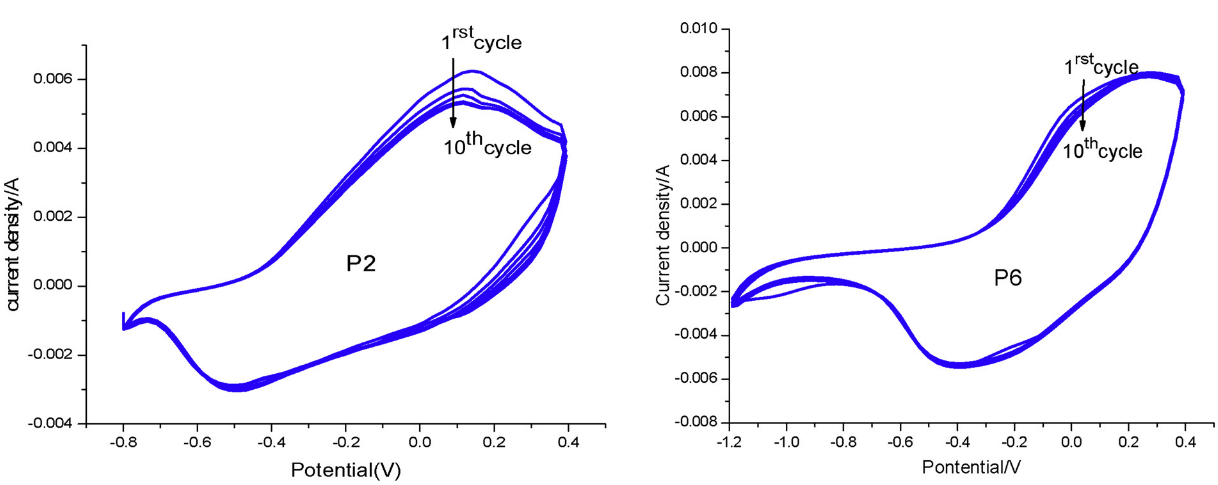

Fig. 9. Cyclic voltammogram of PPy film in free monomer solution: P2) 0.05 M CSA, P6) 0.05 M CSA and 0.03 M Na_2MoO_4, scan rate of 10 mV/s.

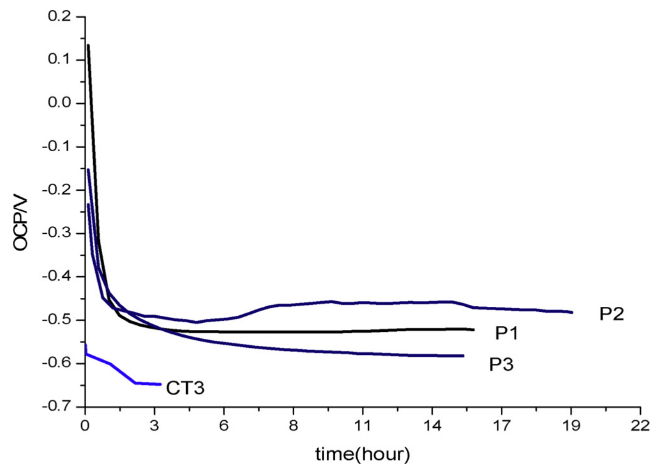

Fig. 10. OCP of samples CT3, P1, P2, and P3 in 3% NaCl solution.

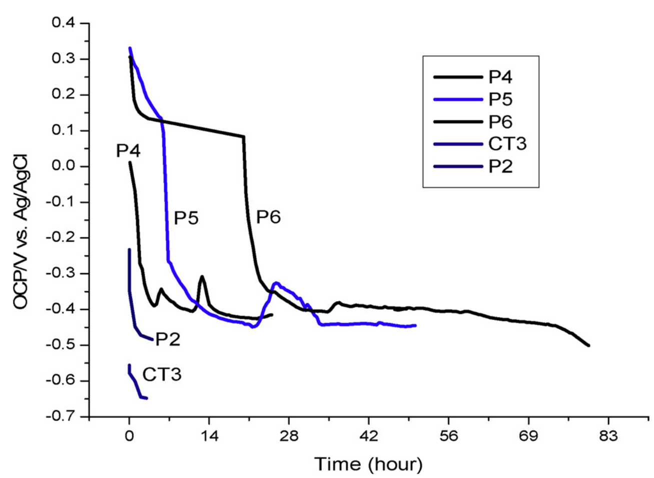

Fig. 11. OCP of samples CT3, P2, P4, P5, and P6 in 3% NaCl solution.

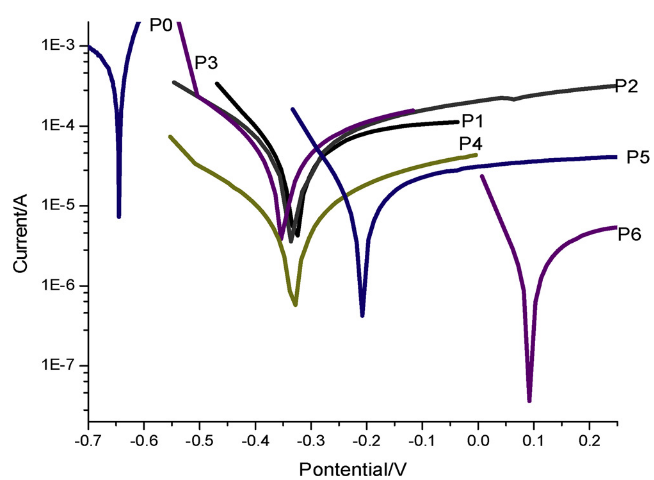

Fig. 12. Tafel curves of samples CT3 (P0), P1, P2, P3, P4, P5, and P6 in 3% NaCl solution.

3.6. Thermogravimetric analysis of doped PPy films

Similar to the EDX analysis, TGA analysis was performed only on the P2, P4, P5 and P6 samples and their TGA and DTA curves are presented in Fig. 8. The doped PPy films were degraded through many steps corresponding to the multiphase structure of these films (PPy, CSA, MoO_4^{2-}, residual monomer, oligomers and other impurities). For instance, the weight loss caused by the evaporation of water occurred in the range of 20 − 100 °C. Next, the degradation of residual monomer, oligomers, CSA and other impurities occurred at 100–400 °C. The weight loss at 400–600 °C was attributed to the decomposition of PPy. The CSA-PPy film was degraded completely at 600 °C, while the MoO_4^{2-}-CSA-PPy films were decomposed partially, from 51.1 to 80.6 wt.% at 600 °C (see Table 4). This difference can be explained by the presence of molybdate anions leading to the formation of passive layers on the CT3 steel surface. As a result, the polymerization of pyrrole monomers was prevented and the obtained PPy in MoO_4^{2-}-CSA-PPy films had a smaller molecular weight in comparison with the CSA-PPy film. On the other hand, the molybdate anions had a high thermal stability at 600 °C and played the role of a physical barrier layer to prevent the penetration of heat and oxygen into the structure of the samples; therefore, the weight of the residue char increased at 600 °C corresponding to the enhancement of the thermal stability of the samples by the presence of molybdate anions.

For the P4, P5, and P6 samples, one more step of degradation can be seen at a temperature above 700 °C, caused by the degradation of MoO_4^{2-} to MoO_3. The weight of the solid which was not degraded (MoO_3) was 15.94, 19.90, and 40.33% for the P4, P5, and P6 films, respectively (Table 4). From these results, it was clear that the doping yield of molybdate anions in the CSA-PPy films for the P6 sample is the highest among the 3 investigated samples. This will be related to the corrosion resistance ability of the doped PPy films as will be discussed below.

3.7. Electrochemical oxidation and reduction of PPy film

The electrochemical redox behavior of PPy films was studied with cyclic voltammetry (CV). The CV of PPy film was obtained in free monomer solution and shown in Fig. 9.

The CV of PPy film (Fig. 9, P6) showed a pair of strong and broad peaks of reduction and oxidation in the presence of Mo in the solution. The oxidation and reduction peaks were assigned at 0.0 V and −0.4 V, respectively. It could be observed that the redox peak of the PPy film was shifted to a more negative direction in CSA solution, i.e., 0.1 V and −0.5 V for oxidation and reduction, respectively (Fig. 9, P2). After 10 cycles, the PPy film was stable with good adhesion on the passivated mild steel. There was no evidence of the destruction of the film.

During the potential scanning, PPy was oxidized and reduced continuously. The incorporation and release of anions have been shown on the CV graphs. The CSA and MoO_4^{2-} anions were mobile enough to go in/out to/from the PPy film. The redox peak could be obtained easily. However, PPy doped with only CSA (P2) was more difficult to be oxidized and reduced when compared to PPy doped with both MoO_4^{2-} and CSA (P6). The oxidation and reduction peaks of P2 were more positive and more negative than that of PPy doped with both MoO_4^{2-} and CSA, respectively. In the presence of both CSA and MoO_4^{2-}, it seemed that the PPy film was reduced easily as shown by one reduction peak (Fig. 9, P6). Both these dopants could be released from the PPy film at the same time.

3.8. Electrochemical study for the corrosive protection of doped PPy film on CT3 mild steel substrate

The open circuit potential (OCP) of the PPy samples was obtained in 3% NaCl electrolyte. The CT3 substrate was passivated in a 0.1 M Na_2MoO_4 solution before measuring the OCP in 3% NaCl solution. The OCP-time curves are shown in Figs. 10 and 11.

The OCP curves of P1, P2, P3 and CT3 exhibited nearly the same behavior. They were positive at the beginning and dropped down after a certain time. When the OCP goes down to the corrosion potential, the PPy coating cannot protect the steel any more. It is clear that in the presence of PPy doped with CSA, the protection time was longer than that of the bare CT3 steel sample (Fig. 10). The P1 and P3 coatings

Table 5
Corrosion potential and current of PPy coatings in 3% NaCl solution.

	CT3 (P0)	P1	P2	P3	P4	P5	P6
i_{corr} (μA cm^{-2})	722	50.5	40.5	47.8	13.4	15.7	3.08
U_{corr} (V) vs. Ag/AgCl)	−0.645	−0.325	−0.320	−0.350	−0.330	−0.206	0.098
η(%)	–	93.0	94.4	93.4	98.1	97.8	99.6
CR (meter per year)	0.00848	0.00059	0.00048	0.00056	0.00016	0.00018	0.00004

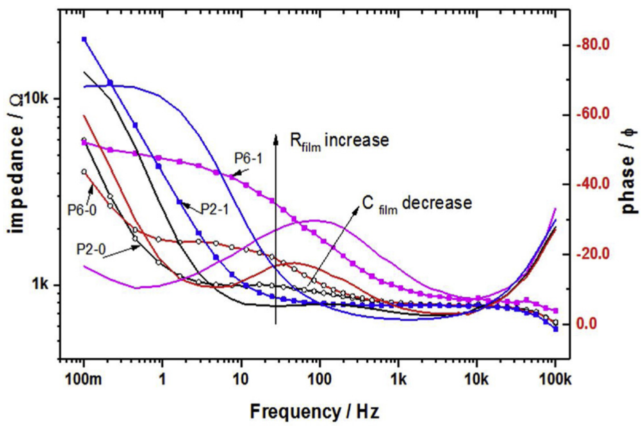

Fig. 13. EIS of samples P2 and P6 obtained in 3% NaCl solution: Samples P2 and P6 at the beginning of immersion (P2-0, P6-0); samples P2, P6 after 1 h of immersion (P2-1, P6-1).

could provide a barrier protection for steel during the immersion time. The OCP of the P2 sample showed a different change. After 7 h, the OCP was shifted to a positive value and prolonged to 16 h. This could be explained by that the resistance of the coating was improved due to the reduction of PPy-CSA. This is the reason for choosing P2 as a control sample for further investigation.

The OCP behavior of PPy doped with MoO_4^{2-} and CSA (P4, P5, P6) was totally different. The OCP kept a positive value for a certain time before dropping down to the corrosion potential of the steel. The protection time of P4, P5, and P6 was extended to a longer time than that of P2 and CT3. Sometimes, the OCP fluctuated during some periods. Among the investigated samples, P6 had the longest plateau of potential. The OCP leveled off at +0.1 V for a long time, nearly 17 h. This behavior was very special which could only be seen in the PPy film doped with molybdate. This behavior indicated the self-healing ability of the PPy film [32]. Although the CT3 substrate was passivated with molybdate, its OCP reached the corrosion potential in a very short time of exposure in NaCl solution. This behavior of OCP was typical for the self-healing action when molybdate played the role of a dopant. CSA dopants also play an important role in providing anticorrosion ability to PPy film. The synergistic effect of molybdate and CSA could be a reason in the enhanced corrosion protection of PPy coating.

The Tafel curves of the PPy films are shown in Fig. 12. The shifts of the corrosion potential and current of the PPy films are clear in comparison with the bare steel substrate P0. It could be seen in Fig. 12 and Table 5 that the corrosion current of the PPy films was smaller than that

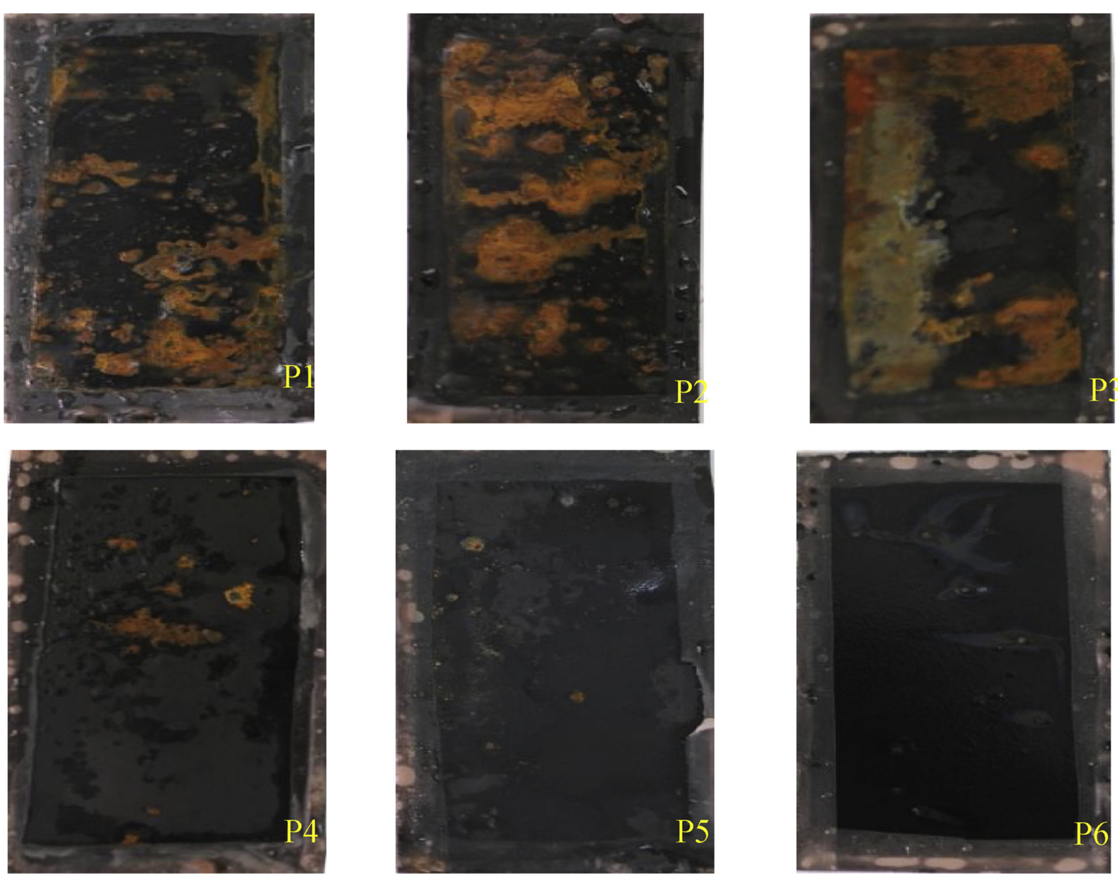

Fig. 14. Salt spray corrosion test of the PPy samples (P1, P2, P3, P4, P5, P6) for 16 h.

of the bare CT3 substrate. All the corrosion potentials trended towards the positive direction. The sample P6 had a corrosion potential of nearly +0.1 V and the corrosion current was the smallest one. The protection efficiency (η) values were obtained according to Eq. 1 and the corrosion rate (CR) was calculated using Faraday's Law (Eq. 2) [39].

$$\eta = \frac{(i_{cor,Fe} - i_{cor,P})}{i_{cor,Fe}} \times 100\% \quad (1)$$

where η is the protection efficiency of the coatings, and $i_{corr,Fe}$, $i_{corr,P}$ are the corrosion current values in the absence and presence of the PPy coating.

$$CR = 3.27 \times 10^{-6} \times (\text{equivalent weight}/\rho) \times i_{corr} \quad (2)$$

where CR is the corrosion rate in meter per year, the equivalent weight of iron is 28 g mol^{-1}, ρ is the density of iron (7.8 g cm^{-3}), and i_{corr} is in Acm^{-2}.

The results of OCP and polarization measurements showed that the PPy ability of corrosion protection could be improved with molybdate and CSA dopants. P6 has the highest corrosion efficiency of 99.6% and lowest corrosion rate of 0.00004 m per year. The self-healing action could be observed with small fluctuations or oscillations and may be due to the passive and/or active process of the pitting. The mobility of molybdate and CSA dopants could be large enough to be released from the PPy film during the protection of CT3 steel. On the other hand, the CSA anion is large and not easily replaced by chloride ion during the corrosion process [39]. Thus, it could provide better corrosion protection ability of PPy. The corrosion ability of the PPy coating was also studied with EIS. Samples P2 and P6 were chosen to compare the film anticorrosion ability in the cases with only the CSA dopant and with both CSA and molybdate dopants in the PPy coating. The change of film resistance was obtained during immersion in 3% NaCl solution. The results are shown in Fig. 13.

With the PPy coating on the steel, the frequency ranging from 10 Hz to 100 Hz in the EIS measurement presents the change of the film resistance [42–44]. The lowest frequency occurs at the highest impedance due to the resistance of charge transfer. As is known from the literature, during immersion of PPy/steel coating in a corrosion medium, the PPy would be reduced due to galvanic coupling. In Fig. 13, the change of the film resistance during immersion is marked with an arrow. The increase of impedance could be seen with the decrease of capacitance of the PPy film, also marked with an arrow (R_{film} increase). The phase angle shifted towards a more negative direction in this range of frequency. At the beginning, the PPy films P2 and P6 (P2-0; P6-0) were in the oxidized state so that the conductivity of the films was very high or the resistance of the films was very small. The resistive behavior could be seen with the phase shift being nearly zero. In the presence of both CSA and molybdate, the resistance of the film was larger (P6-0) than that of the film containing only CSA (P2-0).

During immersion, the film resistance of P2 could reach 1 kOhm (P2-1) and that of P6 (P6-1) could reach 5 kOhm. The PPy films were reduced. The change of film resistance would be an evidence for the self-repairing ability of PPy. The capacitive behavior of the PPy film was presented with the rise of the phase shift to nearly −30°. The mobility of both CSA and molybdate dopants seemed good enough to be released from the PPy film at the same time. This could be a reason that the phase angle shift of P2 was smaller than that of P6 during immersion. Due to the synergistic effect of both CSA and molybdate dopants, the PPy film has a better resistance.

The samples were tested after 16 h of exposure to a salt spray (Fig. 14). The sample P6 showed no corrosion point and a small blister. The samples without molybdate (P1, P2, P3) displayed a serious attack of approximately 60–75% of the total area, whereas the steel sample coated with PPy at the same time of the spray did not. In P3, the blister was large, nearly 50% of the sample area. P5 and P6 presented excellent adhesion to the substrate after 16 h of salt spray testing and nearly no underlayer corrosion was found. It could be observed that the PPy film could provide corrosion ability for mild steel in the presence of both molybdate and CSA. Both could act as mobile inhibitor dopants. The mechanism of the corrosion protection by PPy doped with MoO_4^{2-} has already been discussed in many papers [42,44]. The release of CSA and MoO_4^{2-} during the protection time (reduction reaction) could be seen as the main mechanism.

4. Conclusions

In this work, polypyrrole (PPy) film was electrodeposited successfully on a CT3 mild steel substrate in the presence of both molybdate anions and 10-camphorsulfonic acid (CSA) as dopants. The molybdate anions and CSA played an important role in the passivation of the mild steel substrate which helped to obtain a smooth film and adherence. The PPy film was stable and there was no evidence of film destruction after 10 cycles of potential scanning. The molybdate anions contributed to improving the thermal stability of the doped PPy films. Although the CSA mobility was smaller than that of the molybdate anion, it could be released slowly from the PPy film during reduction. The molybdate anion and CSA dopants could enhance the protection of PPy with self-healing and barrier properties. These obtained results show that PPy film doped with both CSA and molybdate anions could act as a promising corrosion protection coating.

References

[1] C.H. Chang, T.C. Huang, C.W. Peng, T.C. Yeh, H.I. Lu, W.I. Hung, C.J. Weng, T.I. Yang, J.M. Yeh, Novel anticorrosion coatings prepared from polyaniline/graphene composites, Carbon 50 (14) (2012) 5044–5051.
[2] L. Zhang, W. Du, A. Nautiyal, Z. Liu, X. Zhang, Recent progress on nanostructured conducting polymers and composites: synthesis, application and future aspects, Sci. China Mater. 61 (3) (2018) 303–352.
[3] C. Li, K. Mitamura, T. Imae, Electrostatic layer-by-layer assembly of poly(amido amine) dendrimer/conducting sulfonated polyaniline: structure and properties of multilayer films, Macromolecules 36 (26) (2003) 9957–9965.
[4] T. Jin, F. Zhang, Interaction mechanism of ultrafine silica and poly(amido-amine) and dispersibility of the complexes in coatings, Prog. Org. Coat. 72 (2–3) (2013) 447–451.
[5] I.L. Lehr, S.B. Saidman, Bilayers polypyrrole coatings for corrosion protection of SAE 4140 steel, Port. Electrochim. Acta 32 (4) (2014) 281–293.
[6] L. Zhang, S. Liu, H. Han, Y. Zhou, S. Hu, C. He, Q. Yan, Studies on the formation process and anti-corrosion performance of polypyrrole film deposited on the surface of Q235 steel by an electrochemical method, Surf. Coat. Technol. 341 (2018) 95–102.
[7] N. Sheng, Y. Lei, A. Hyonoo, M. Ueda, T. Ohtsuka, Improvement of polypyrrole films for corrosion protection of zinc-coated AZ91D alloy, Prog. Org. Coat. 77 (2014) 1724–1734.
[8] H. Shokry, Corrosion protection of mild steel electrode by electrochemical polymerization of acrylamide, Chem. Met. Alloys 2 (2009) 202–210.
[9] T. Tuken, B. Yazici, M. Erbil, The electrochemical synthesis and corrosion performance of polypyrrole on brass and copper, Prog. Org. Coat. 51 (2) (2004) 152–160.
[10] T. Tuken, B. Yazici, M. Erbil, The use of polyindole for prevention of copper corrosion, Surf. Coat. Technol. 200 (16–17) (2006) 4802–4809.
[11] T.D. Nguyen, M.C. Pham, B. Piro, J. Aubard, H. Takenouti, M. Keddam, Conducting polymers and corrosion PPy-PPy-PDAN composite films: electrosynthesis and characterization, J. Electrochem. Soc. 151 (6) (2004) 325–330.
[12] G. Paliwoda-Porebska, M. Stratmann, M. Rohwerder, K. Potje-Kamloth, Y. Lu, A.Z. Pich, H.J. Adler, On the development of polypyrrole coatings with self-healing properties for iron corrosion protection, Corros. Sci. 47 (12) (2005) 3216–3233.
[13] D. Kowalski, M. Ueda, T. Ohtsuka, Corrosion protection of steel by bi-layered polypyrrole doped with molybdophosphate and naphthalenedisulfonate anions, Corros. Sci. 49 (3) (2007) 1635–1644.
[14] H. Nguyen Thi Le, B. Garcia, Q. Le Xuan, C. Deslouis, Corrosion protection of iron by polystyrenesulfonate-doped polypyrrole films, J. Appl. Electrochem. 32 (1) (2002) 105–110.
[15] I.L. Lehr, S.B. Saidman, Characterisation and corrosion protection properties of polypyrrole electropolymerised onto aluminium in the presence of molybdate and nitrate, Electrochim. Acta 51 (16) (2006) 3249–3255.
[16] M.B. González, S.B. Saidman, Electrodeposition of bilayered polypyrrole on 316 L stainless steel for corrosion prevention, Prog. Org. Coat. 78 (2015) 21–27.
[17] F. Li, L. Guo-xi, J. Zeng, G. Gui-hong, Molybdate-doped copolymer coatings for corrosion prevention of stainless steel, J. Appl. Polym. Sci. 131 (16) (2014) 40602.
[18] Z. Chen, W. Yang, B. Xu, Y. Guo, Y. Chen, X. Yin, Y. Liu, Corrosion behaviors and physical properties of polypyrrole-molybdate coating electropolymerized on carbon steel, Prog. Org. Coat. 122 (2018) 159–169.
[19] W. Guixiang, C. Nana, Z. Xiaohong, Z. Lili, Corrosion properties of the polypyrrole-

molybdate film electro-polymerized on the AZ31 Mg alloy, Rare Metal Mat. Eng. 46 (6) (2017) 1480–1485.
[20] J.E. Osorio-Fuente, C. Gómez-Yáñez, M. de los Á. Hernández-Pérez, F. Pérez-Moreno, Camphor sulfonic acid-hydrochloric acid xodoped polyaniline/polyvinyl alcohol composite: synthesis and characterization, J. Mex. Chem. Soc. 58 (1) (2014) 52–58.
[21] A. Nautiyal, M. Qiao, T. Ren, H. Tung-Shi, X. Zhang, J. Cook, M.J. Bozack, R. Farag, High-performance engineered conducting polymer film towards antimicrobial/anticorrosion applications, Eng. Sci. 4 (2018) 70–78.
[22] A. Kumar, R.K. Singh, K. Agarwal, R. Singh, Effect of p-toluenesulfonate on inhibition of overoxidation of polypyrrole, J. Appl. Polym. Sci. 130 (15) (2013) 434–442.
[23] S. Min-Kyu, K. Young-Taek, K. Bum-Seok, J. Kim, K. Char, R. Hee-Woo, Synthesis and characterization of soluble polypyrrole doped with alkylbenzenesulfonic acids, Synth. Met. 141 (3) (2004) 315–319.
[24] J. Hazarika, A. Kumar, Studies of structural, optical, dielectric relaxation and ac conductivity of different alkylbenzenesulfonic acids doped polypyrrole nanofibers, Physica B Condens. Matter 481 (2016) 268–279.
[25] S.T. Navale, A.T. Mane, A.A. Ghanwat, A.R. Mulik, V.B. Patil, Camphor sulfonic acid (CSA) doped polypyrrole (PPy) films: Measurement of microstructural and optoelectronic properties, Measurement 50 (2014) 363–369.
[26] M.A. Chougule, S. Sen, V.B. Patil, Polypyrrole–ZnO hybrid sensor: effect of camphor sulfonic acid doping on physical and gas sensing properties, Synth. Met. 162 (17–18) (2012) 1598–1603.
[27] L. Jiang, J.A. Syed, Y. Gao, Q. Zhang, J. Zhao, H. Lu, X. Meng, Electropolymerization of camphorsulfonic acid doped conductive polypyrrole anticorrosive coating for 304SS bipolar plates, Appl. Surf. Sci. 426 (2017) 87–98.
[28] L. Qu, G. Shi, J. Yuan, G. Han, F. Chen, Preparation of polypyrrole microstructures by direct electrochemical oxidation of pyrrole in an aqueous solution of camphorsulfonic acid, J. Electroanal. Chem. 561 (2004) 149–156.
[29] K. Krukiewicza, A. Katunin, The effect of reaction medium on the conductivity and morphology of polyaniline doped with camphorsulfonic acid, Synth. Met. 214 (2016) 45–49.
[30] J.E.P. da Silva, S.I.C. de Torresi, R.M. Torresi, Polyaniline acrylic coatings for corrosion inhibition: the role played by counter-ions, Corros. Sci. 47 (3) (2005) 811–822.
[31] H. Ryu, N. Sheng, T. Ohtsk, S. Fujita, H. Kajiyama, Polypyrrole film on 55% Al–Zn-coated steel for corrosion prevention, Corros. Sci. 56 (2012) 67–77.
[32] V.Q. Trung, P.V. Hoan, D.Q. Phung, L.M. Duc, L.T.T. Hang, Double corrosion protection mechanism of molybdate-doped polypyrrole/montmorillonite nanocomposites, J. Exp. Nanosci. 9 (3) (2014) 282–292.
[33] I.L. Lehr, S.B. Saidman, Characterisation and corrosion protection properties of polypyrrole electropolymerised onto aluminum in the presence of molybdate and nitrate, Electrochim. Acta 51 (16) (2006) 3249–3255.
[34] K.M. Cheung, D. Bloor, G.C. Stevens, Characterization of poly-pyrroleelectropolymerized on different electrodes, Polymer 29 (9) (1998) 1709–1717.
[35] M.J.L. Santos, A.G. Brolo, E.M. Girotto, Study of polaron and bipolaron states in polypyrrole by in situ Raman spectroelectrochemistry, Electrochim. Acta 52 (20) (2007) 6141–6145.
[36] A. Faulques, W. Wallnoefer, H. Kuzmany, Vibrational analysis of heterocyclic polymers: a comparative study of polythiophene, polypyrrole, and poly-isothianaphtene, J. Chem. Phys. 90 (12) (1989) 7585–7593.
[37] V.Q. Trung, D.N. Tung, D.N. Huyen, Polypyrrole/Al_2O3nanocomposites: preparation, characterization and electromagnetic shielding properties, J. Exp. Nanosci. 4 (3) (2009) 213–219.
[38] V.Q. Trung, T.H. Hanh, T.H. Quang, H.M. Hung, D.K. Linh, H.T.T. Lan, L.M. Duc, Corrosion protection of molybdate doped polypyrrole film prepared in succinic acid solution, Corros, Eng. Sci. Techn. 53 (S1) (2018) 59–66.
[39] A. Nautiyal, M. Qiao, J.E. Cook, X. Zhang, T.S. Huang, High performance polypyrrole coating for corrosion protection and biocidal applications, Appl. Surf. Sci. 427 (part A) (2018) 922–930.
[40] D.E. Tallman, K.L. Levine, C. Siripirom, V.G. Gelling, G.P. Bierwagen, S.G. Croll, Nanocomposite of polypyrrole and alumina nanoparticles as a coating filler for the corrosion protection of aluminum alloy 2024-T3, Appl. Surf. Sci. 254 (17) (2008) 5452–5459.
[41] J.M. Yeh, C.P. Chin, S. Chang, Enhanced corrosion protection coatings prepared from soluble electronically conductive polypyrrole-clay nanocomposite materials, J. Appl. Polym. Sci. 88 (14) (2003) 3264–3272.
[42] U. Rammelt, L.M. Duc, W. Plieth, Improvement of protection performance of polypyrrole by dopant anions, J. Appl. Electrochem. 35 (12) (2005) 1225–1230.
[43] G. Paliwoda-Porebska, M. Rohwerder, M. Stratmann, U. Rammelt, L.M. Duc, W. Plieth, Release mechanism of electrodeposited polypyrrole doped with corrosion inhibitor anions, J. Solid State Electrochem. 10 (9) (2006) 730–736.
[44] W. Plieth, A. Bund, U. Rammelt, S. Neudeck, L.M. Duc, The role of ion and solvent transport during the redox process of conducting polymers, Electrochim. Acta 51 (11) (2006) 2366–2372.